Research Square

Preprints are preliminary reports that have not undergone peer review.
They should not be considered conclusive, used to inform clinical practice,
or referenced by the media as validated information.

Does Soil Health Have a Tipping Point?

John W. Crawford

john.crawford@glasgow.ac.uk

University of Glasgow

Aurélie Bacq-Labreuil

Rothamsted Research

Cris Hasan

University of Glasgow

Stuart Kauffman

Institute for Systems Biology

Sacha J. Mooney

University of Nottingham

William Rickard

Rothamsted Research

Iain M. Young

King Abdullah University of Science and Technology

Xiaoxian Zhang

Rothamsted Research

Andrew L. Neal

Rothamsted Research

Article

Keywords: self-organisation, soil carbon, resilience, climate change, food security, water security

Posted Date: November 10th, 2026

DOI: https://doi.org/10.21203/rs.3.rs-11361432/v1

License: This work is licensed under a Creative Commons Attribution 4.0 International License.
Read Full License

Additional Declarations: No competing interests reported.

Does Soil Health Have a Tipping Point?

John W. Crawford*[,1], Aurélie Bacq-Labreuil[3], Cris Hasan[2], Stuart Kauffman[4], Sacha J. Mooney[5], William Rickard[6], Iain M. Young[7], Xiaoxian Zhang[8], Andrew L. Neal[9]

1. School of Geographical and Earth Sciences, University of Glasgow, Glasgow G12 8QQ. UK, and the George Town Institute of Open and Advanced Studies, Wawasan Open University, 54, Jalan Sultan Ahmad Shah 10050 Penang, Malaysia
2. Adam Smith Business School, University of Glasgow, Glasgow G12 8QQ. UK
3. Greenback SA (commercial name: Genesis), Paris, 75003, France
4. Institute for Systems Biology, Seattle, WA, USA
5. Division of Agriculture & Environmental Sciences, School of Biosciences, University of Nottingham, Sutton Bonington Campus, Leicestershire LE12 5RD, UK
6. Soil Health and Management, Rothamsted Research, Harpenden, Herts, AL5 2JQ, UK
7. Biological and Environmental Science and Engineering Division, King Abdullah University of Science and Technology, Thuwal 23955-6900, Kingdom of Saudi Arabia
8. Net-Zero and Resilient Agriculture, Rothamsted Research, North Wyke EX20 2SB, UK

* Corresponding author: john.crawford@glasgow.ac.uk

Abstract.

Soil degradation contributes significantly to climate change, biodiversity loss, and threatens food and water security worldwide. Studies indicate that increasing soil organic carbon can restore vital soil functions and substantially lower atmospheric CO_2 levels when scaled globally. However, large-scale investment in soil is limited by uncertainties about how inputs impact the resilience and stability of carbon stocks and biophysical functioning. Building on earlier research, we propose a general theory of the soil-microbe ecosystem that links soil type and management to the resilience of carbon stocks and key soil functions. Data from extensive long-term experiments across six soil types and eighteen different management practices are consistent with the emergence of a self-organised critical state with a critical 'tipping' point governed by organic carbon. A common set of parameters for the dynamical state describes all but the sandiest soils (>60%), suggesting universal behaviour across the other soils and management practices studied. The sandiest soil shows no evidence of a self-organised critical state. Near the critical point, small changes in soil carbon stocks result in large shifts in soil physical and biological function. Tillage and reduced organic inputs tend to push soils toward this tipping point, but the self-organised critical state helps stabilise carbon stocks and sustain biological functioning when carbon inputs fluctuate. Recovery from a degraded state beings soon after management is improved, but restoring the original critical state takes at least a decade, and dynamical equilibrium is only achieved decades after that. These findings provide a framework for understanding degradation and recovery of the soil-microbe system, identifying carbon thresholds and evaluating the timescales required to rebuild soil resilience, pointing towards a possible general theory for soil ecosystems.

Key words: self-organisation, soil carbon, resilience, climate change, food security, water security

Introduction

It is widely agreed that restoring soil health is a global priority to ensure future food and water security, support biodiversity, and to mitigate and adapt to climate change[1,2,3]. Soil organic carbon content has emerged as a common proxy for soil health[4] and has therefore become an important target for nature-based solutions. Consequently, there is a growing number of programmes that aim to accelerate the restoration of soil health at scale, driven by the potential return on investment from carbon offsetting or insetting and by higher and/or more stable yields from lower inputs, even though outcomes cannot be generalised[5].

There is a scientific consensus on four standard strategies to increase soil organic carbon content and, by extension, improve soil health – minimising soil disturbance, maximising soil coverage, increasing crop diversity, and applying organic amendments[6,7,8]. These are high-level recommendations and therefore require translation to local conditions before they can be operationalised. This translation step can't yet be generalised because there are many possible combinations of management practices, cropping systems, soil types, and environmental and human factors, which means that most scientific knowledge has limited practical relevance for farmers[5,76,87,9].

Aside from these practical limitations, the main impediments to large-scale investment in soil carbon relate to uncertainties in the return on investment e.g. the cost of measuring soil carbon[10], uncertainty in the resilience of carbon stocks to external shocks[11,12], and the level of investment where financial and functional benefits level off[13]. Furthermore, there is debate on the potential and practical contribution to mitigating climate change[14,15]. With an improved understanding of how management, carbon dynamics, soil function, and resilience are related, more cost-effective measurement methods can be developed, risks can be better managed, and interventions can be designed to optimise a broader range of outcomes[10]. Achieving this requires a new general theory for soil health that provides the required synthesis of these exogenous and endogenous factors. We present such a theory here, and provide empirical and theoretical evidence to support it.

Soil Health and Dynamical Systems Theory.

The general concept of health relates to the dynamical state of life-supporting functions maintained through internal feedback processes that maintain a stable state or restore the system's characteristic trajectory after external perturbation[4]. These properties are usually an emergent outcome of a dynamical system comprising non-linear interactions between physical and biological components. For soil, there is currently no general dynamical systems theory on which to base the concept of health[16,17]. However, we note that key soil properties, including microbial activity, nutrient cycling, plant productivity, carbon dynamics, and GHG emissions, are all emergent outcomes of the soil's capacity to maintain a mixture of air and water within an interconnected pore space across a wide range of environmental conditions[18,19,202120]. This fundamental property is a consequence of the geometry of the soil pores of diameter approximately less than 50μm that hold water against gravity and control oxygen movement to microbial microsites, particularly the total volume of these pores and their degree of connectedness. We use high-resolution μ-CT to measure and analyse soil structure at these scales.

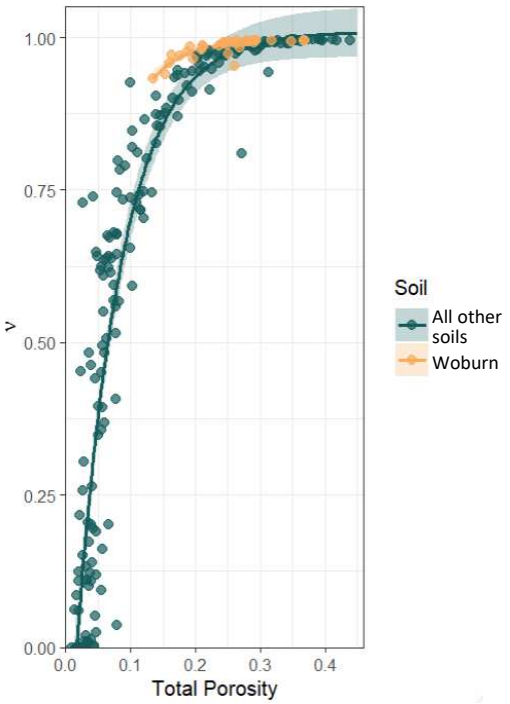


Figure 1. The same critical behaviour is observed across different management in low sand content soils, but not in high sand content soil. The proportion, (v), of connected porosity to the total porosity, (P_t), is plotted as a function of P_t in 2-mm sized aggregates scanned at 1.5-µm resolution using X-ray computed tomography. There is a strong and non-linear response of connected porosity to changes in P_t in soils with a low sand content (from the Highfield Ley-Arable, $n = 32$ and Highfield reversion experiments, $n = 107$ with 13% *w/w* sand, soil from the Broadbalk Winter Wheat experiment with 25% w/w sand, $n = 42$, soil the the Longlands fields of the North Wyke Farm Platform with 22% *w/w* sand, $n = 67$, and soil from plots at FarmED with 24% w/w sand, $n = 28$). In contrast, there is a weakly non-linear response and no evidence for a critical value of P_t in soil with a high sand content (from the Woburn Organic Manuring long-term experiment with 70% *w/w* sand, $n = 35$). Fitted curves are of the form $v = v_\infty(1-\exp(-K(P_t-t_0)))$ where v_∞ represents the upper limit of pore connectivity (i.e., 1), P_t represents total porosity, and t_0 represents the theoretical total porosity when v equals zero. Goodness-of-fit of the model to low sand content soils, $r^2 = 0.858$, $n = 182$, and for high sand content soils, $r^2 = 0.729$, $n = 35$.

There is evidence that the organisation of soil particles is not random but has scale-free spatial correlations that can be approximated using fractal geometry[21,22]. There is no accepted theory for the dynamical origins of pore space geometry, but it has been proposed that the interaction between microbial activity, particle aggregation, and substrate diffusion results in self-organisation[23,24]. The hypothesis behind this proposal is that particle associations adjacent to a location of higher microbial activity are reinforced against disruption preferentially (e.g., by wet-dry cycles) compared with particles in locations with lower or zero microbial activity. The proposed reinforcing agents are by-products of microbial metabolism, including extracellular polymeric substances and necromass binding to charged surfaces. A simple particle aggregation model[25] predicts this results in the emergence of a non-random pore geometry, i.e. a higher pore volume and more connected pore space than would occur otherwise in the absence of such interactions. This prediction is supported by laboratory- and field-based experimentation[26,27,25,20].

Self-organisation is generally challenging to prove, and its role in the soil microbe system remains a conjecture. Some of the strongest evidence of self-organisation in any system is the observation of self-organised critical behaviour (SC) i.e. the existence of a critical (or tipping) point and internal dynamics that maintain the system close to the critical point. This is evidenced by the system satisfying the following four conditions:

(1) the presence of a critical point i.e. the value of a control variable where the properties of the system change discontinuously, such as at the freezing point of water;
(2) power-law scaling of system parameters close to the critical point, meaning large system-wide compensatory changes occur in response to external forcing of the control variable [28];
(3) internal processes that maintain the control variable in the vicinity of the critical value;
(4) oscillations and complex transient dynamics following perturbation when the system is close to the critical point.

In this paper, we provide evidence for SC in soil in the form of data, analysis, and modelling corresponding to the conditions (1)-(4) in the following sections and then discuss the consequences of SC for our understanding of soil health and alleviating the impediments to investment.

Evidence of a critical/tipping point and power-law behaviour

We use a data-driven approach to search for evidence that conditions 1 and 2 for SC are met in our study soils[29]. While SC provides strong evidence for self-organisation in soil, it also yields insight into the underlying dynamical state related to the concept of health in other living systems[30]. The most relevant paradigm for SC in soil is percolation theory[31]. This relates to the spontaneous emergence of system-wide organisation in random lattices of nodes and links, known as percolation clusters, as the link density approaches a critical value. This critical value, called the percolation threshold, marks the point at which the lattice transitions from disconnected (no pathway of connected nodes spans the lattice) to connected (at least one connected pathway exists). Percolation theory has been used to understand a wide range of phase transitions in biological, chemical, and physical phenomena and has previously been applied to soil[32,33].

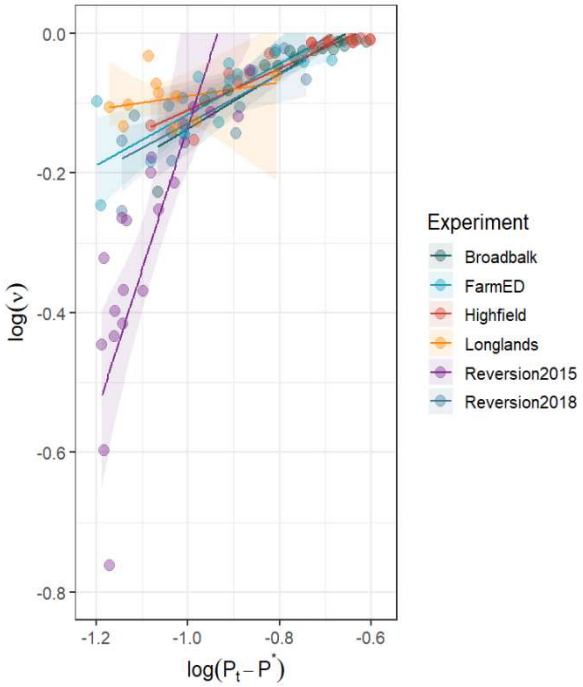


Figure 2. Power-law exponents characterise behaviour close to the tipping point. Log-log plot of v vs. the deviation of the total porosity from P^*. Data from soils collected from the Broadbalk Winter Wheat experiment (r^2 = 0.787, n = 17), Highfield Ley-Arable experiment (r^2 = 0.859, n = 13), the Highfield Reversion experiment (2015 r^2 = 0.627, n = 7, 2018 r^2 = 0.511, n = 14), Longlands fields of the North Wyke farm platform (r^2 = 0.073, n = 10) and plots of FarmED (r^2 = 0.597, n = 14).

We can relate percolation theory to soil by conceptualising a three-dimensional structure comprised of voxels that are either pore space or solid. Defining P as the probability that a random voxel is pore space, being equivalent to the porosity of the soil, then there exists a critical value of P, (P^*) whereby the pore space switches from being connected to disconnected. Close to P^*, the porosity and rate coefficients of associated transport processes (such as diffusion and convection rates) scale as power laws of P. At and below P^*, the transport coefficients are zero. The critical point, P^*, is often referred to as a tipping point of the system[34]. Jarvis et al. analysed 64µm resolution µ-CT images of a silt loam soil and provided evidence for a critical point[33] with a value of P^* in the range 4% to 6%. They noted that the pore network characteristics were not significantly impacted by cropping treatments or sampling year. Soto-Gomez et al estimated a percolation threshold of 1.4%±1.4% for a sandy soil imaged using µ-CT at resolution 240µm, pointing out that this was significantly lower than the percolation threshold for random structures.

We studied the pore space geometry in soil from five contrasting experimental systems managed by Rothamsted Research and a demonstration farm, all located in southern England. The detailed methodology is described in the Supplementary Material. The soils differed in texture (*i.e.*, particle size distribution) and were subject to different nutrient management, planted crop, and tillage practices. The first was the Broadbalk Winter Wheat Experiment (geolocation 51.80946, -0.37301), which had been ploughed and planted with wheat every year since 1843. We selected five contrasting management and nutrient amendment treatments: organic (FYM), conventional with added nitrogen, potassium, and phosphorus (144NPK), conventional but with no added phosphorus (193NK), no added nutrients (nil), and rewilded since 1882 (woodland). The field experiment is described in more detail in Neal *et al*.[35]. The second was the Highfield Ley-Arable Experiment (geolocation 51.802777, -0.366025), which had been running for 74 years at the time of sampling and where there were three cropping treatments: bare fallow (soil that had remained unplanted with zero input of nutrients, except through rainfall, since 1959); permanent grassland (pasture); and continuous wheat (240NPK). Both grassland and wheat treatments had added inorganic nutrients, and the wheat treatment had been ploughed each year. The Highfield Ley-Arable experiment is described in more detail by Neal *et al*.[20]. The third experiment was the Highfield Reversion Experiment, where in 2007 several plots of the bare fallow treatment referred to above were planted with either wheat or grass, and otherwise managed in the same way as the permanent grass and wheat treatments. The reversion plots are described in detail elsewhere[36] in. The fourth experiment was the Woburn Organic Manuring Experiment (geolocation 51.999805, -0.616036), which has been managed since 1964 in a similar way to the Broadbalk Experiment, but on soil with a much higher sand content. This experiment and historical data related to it are described by Johnston *et al*.[37]. The fifth experiment sampled soils from the fields Longlands North, Longlands East, and Longlands South of the North Wyke Farm Platform (geolocation 50.772369, -3.902470), established in 2010 on existing grassland. At the time of sampling fertility of Longlands South was managed by inorganic fertilisation, nitrogen fertilisation was replaced on Longlands North by re-seeding with legumes every three or four years, and after a period of management as pasture, since 2019 Longlands East was managed as inorganically fertilised arable and ploughed to a depth of 30 cm each year. A complete description of the farm platform and fields within it is provided by Hawkins *et al*.[38]. The sixth field experiment was situated at FarmED; (geolocation 51.869671, -1.581625), a demonstration farm in the south of England. Since 2014, eight strips of approximately 0.8 ha each have been managed in a staggered eight-year rotation (four years of multi-species herbal ley followed by four years of cereals), with each strip at a different rotational stage in any given year. The herbal leys comprised five grass species, seven legume species, and six herb species, grazed by sheep and terminated by inversion tillage. Two additional plots, a 0.96-ha continuous no-till cereal plot (no-till annual) and an approximately 3-ha long-term (LT) organic permanent pasture (perennial-LT), served as examples of annual cereal cropping in the absence of herbal leys and long-term perennial management. Prior to 2014, all rotation and no-till plots were managed as tilled, inorganically fertilised continuous arable. We sampled soil from the permanent cereal and pasture, from a four-year-old herbal ley and from soil six weeks after herbal ley termination by inversion tillage and power harrowing. The soils included in the study exhibited a broad range in sand (particle size, 50 – 2,000 μm) content by mass, from 13%, to 70%.

Replicate 2-mm sized aggregates taken from soils in all treatments and experiments were imaged in three dimensions using X-ray Computed Tomography using previously published protocols20 with 1.5-µm nominal resolution, equivalent to a 3-µm² feature resolution in 2-D, or a 27-µm3 feature resolution in 3-D.

Figure 1 shows a plot of the ratio (denoted hereafter by v) of the connected porosity (P_c) to the total porosity (P_t) for all treatments and replicates in the Highfield, Broadbalk, FarmED, Longlands fields of the North Wyke farm platform, and Woburn experiments. P_t is the porosity calculated from the images and includes only pores larger than the scans' feature resolution. P_c is the porosity of the pore space that connects to the outside of the aggregate. The combined Highfield, Broadbalk, Longlands and FarmED data show that v increases rapidly with P_t, above P^*. The estimated value of P^* (1.7% ± 0.002% standard error) from the combined field estimates was significantly greater than zero (*t*-test, $t = 8.1$, one-tailed $p = 1 \cdot 10^{-13}$), meaning that P_c becomes zero for non-zero values of P_t. Power-law scaling—a characteristic of self-organised critical states[29]—is evident in Figure 2 for soil from the Highfield, Broadbalk, Longlands and FarmED experiments, along with data from 2015 and 2018 from the Highfield Reversion Experiment. Major axis regression identified significant slopes (β) for all soils except those from Longlands ($\beta = 0.097$, $t = 0.791$, $p = 0.452$) suggesting that trends for soils characterised as having relatively low sand contents can be modelled as a power-law, $v \propto |P_t - P^*|^{\beta}$. Comparison of slopes for soils where a significant relationship between $\log(P_t\text{-}P^*)$ and $\log(v)$ was identified indicated a common β for Highfield, Broadbalk, FarmED and Highfield reversion soil collected in 2018 (range 0.299 – 0.395). β associated with Highfield reversion soil collected in 2015 (2.05) was statistically greater than all other soils (smallest difference 1.65 with Broadbalk soil, likelihood ratio = 4.2, Benjamini-Hochberg adjusted $p = 4 \cdot 10^{-8}$). The existence of a critical value for porosity and the power-law behaviour close to this critical value is consistent with these soils being in a self-organised critical state, with P^* reflecting a tipping point. Neither the Woburn experiment nor the 2008–2012 data in the Highfield reversion experiment satisfied these conditions, and so we conclude that there is no evidence for SC in that data. This is discussed later.

The value of P^* for random percolation (simple cubic lattice geometry) is around 31%, much higher than the values we estimated in these soils[39]. Spatial correlations in the packing geometry, such that the probability of a voxel being pore space is higher if a voxel within a correlation length is also pore space, lower the value of the critical probability, and it decreases as the correlation length increases[40]. Our results suggest that SC is responsible for spatial correlations in soil that move the tipping point outside the porosity range for all management practises except for the artificially degraded soil.

Evidence That Carbon is a Control Variable

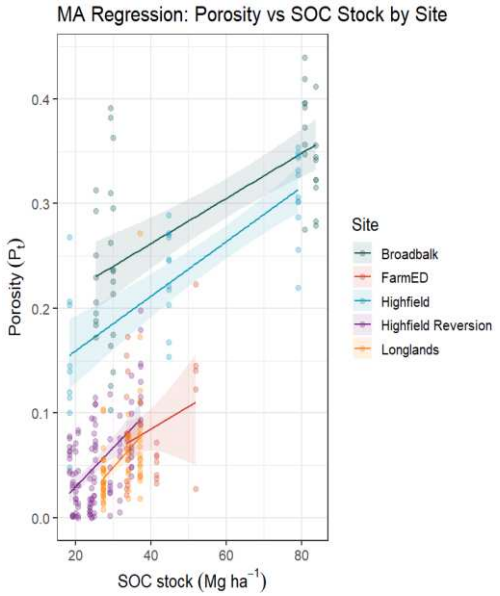


Figure 3*. Data is consistent with a linear dependence of total porosity on soil organic carbon content with slope dependent on texture and/or age of experiment. Plot of P_t vs. soil organic carbon content for soils of the Highfield (n = 32, slope = 0.0026 ± 0.0004, t = 7.3, p = 4·10^{-8}), Broadbalk (n = 42, slope = 0.0022 ± 0.0004, t = 5.6, p = 2·10^{-6}), Highfield reversion (n = 107, slope = 0.0037 ± 0.0007, t = 6.4, p = 4·10^{-9}), Longlands fields of the North Wyke farm platform (n = 67, slope = 0.0041 ± 0.0011, t = 4.0, p = 2·10^{-4}), and plots from FarmED (n = 28, slope = 0.0021 ± 0.0017, t = 1.6, p = 0.128), Note that the same average soil organic carbon content associated with each treatment for soil from each experiment was used as a proxy for the carbon content of each 2-mm replicate.*

Porosity is generally found to be linearly proportional to soil organic matter content[41]. To confirm this for the soils studied here, and so test the hypothesis that P_t is a proxy for carbon as the control variable in our soils, we plotted sample P_t as a function of the average organic carbon content for the different soils and treatments to. Figure 3 shows statistically significant linear relations exist in four of the five experiments and across all treatments despite the considerable variation in porosity values for a given value of the soil organic carbon (likely the result of attributing bulk values of soil carbon in the treatments to porosity values measured from replicate 2 mm aggregates). We observed a common slope describing the relationship between SOC stock and P_t across the five experiments (maximum likelihood slope estimate, 0.0025, likelihood ratio statistic = 8.0, p = 0.093). Therefore, similarly to other studies[42], our results are consistent with porosity being linearly proportional to organic carbon content across the range of carbon stocks observed here. In contrast, there was no statistically significant linear relation between P_t and organic carbon content for soils from the Woburn Experiment (n = 35, slope = 0.0088 ± 0.062, t = 0.141, p = 0.888).

A test for common elevation on the ordinate of Fig. 3 indicated a significant difference in P_t between soils (Wald statistic = 317.0, p = 2·10^{-67}). P_t of soils from the Highfield reversion, FarmED and the Longlands fields were similar, but P_t of Highfield permanent soil and Broadbalk were significantly greater (p = 3·10^{-21} and p = 4·10^{-31}, respectively) than this group. In addition, P_t of Broadbalk soil was significantly greater than that of Highfield plots (p = 0.0014). The consequence of these differences is discussed below.

Evidence that internal processes maintain soil carbon close to the critical value

We use a simple model describing coupling between microbial activity, structure, and carbon stocks and flows to show that Condition 3 for SC is met. We first assume zeroth-order dependence of microbial aerobic respiration[43], and define Q as the potential respiration rate per unit volume (i.e. the respiration rate per unit volume is Q if oxygen is present, or zero otherwise). Then, Q can be interpreted as a proxy for the quantity and/or quality of organic matter in a unit volume of soil. The coupling between structure and microbial activity that is implicated in SC is captured in the model by linking the diffusion rate at a given location in soil to the microbial respiration rate at that location. Formally, this

is expressed in three assumptions: (i) the oxygen diffusion coefficient, D, depends as a power law on porosity[44,20], (ii) a linear relation exists between porosity and soil organic carbon (see Figure 2), and (iii) *Q* is proportional to soil organic carbon content. Under these assumptions, we can write $D \propto Q^k$, with the constant k related to β, the slope of the linear relation between porosity and soil organic carbon content.

The corresponding reaction-diffusion equation can be solved in the steady state, and the derivation is provided in the Supplementary Material. From this solution of this equation, we can relate the steady state soil organic matter content, Q, to the steady state flux of organic matter into the soil system, f, using the following equation,

$$\frac{Q}{Q_0} = \left(\frac{f}{f_o}\right)^{\frac{2}{1+k}}, \qquad (1)$$

Where expressions for the constants f_0 and Q_0 are provided in the Supplementary Material. In the absence of coupling between structure and microbial activity $k = 0$, and the power-law exponent in the equation is equal to 2. Positive values for k correspond to a coupling between microbial activity and structural genesis, which, by assumption, is associated with the self-organised critical state. Larger values of k represent stronger coupling between microbial activity and structure.

Equation 1 shows that SC has contrasting consequences for the equilibrium soil carbon content when the input flux of organic matter is low ($f \ll f_0$) compared to when the input flux is high ($f \gg f_0$). In the former case, SC results in a higher value for the equilibrium soil carbon content, and the equilibrium value increases with k. In the latter case, SC results in a lower soil carbon content that decreases with k.

This simple model therefore predicts that the functional consequence of SC is to stabilise soil organic carbon content when the carbon input is fluctuating. This effect is enhanced when the coupling between soil structure and microbial activity is stronger i.e. for higher values of k. This feedback between system dynamics and the control variable maintains the system in the proximity of the tipping point, which is Condition 3 for SC[29].

Evidence for complex transient dynamics following a perturbation

Finally, we searched for evidence for complex dynamics and transient behaviour following soil perturbation, Condition 4 for SC. We used the example of restoration of degraded soil using data from the Highfield Reversion experiment. Figure 4 shows the relation between v and $\mathrm{P_t}$ for all years for which we have data. There is evidence for both a non-zero value for P^* and a power-law relation of the form $v \propto |P_t - P^*|^\beta$ only after eight years following the initial perturbation. There is no significant difference in the value of β between 2015 and 2018, or between that value and the value for the long-term Highfield and Broadbalk experiments (see Figure 2).

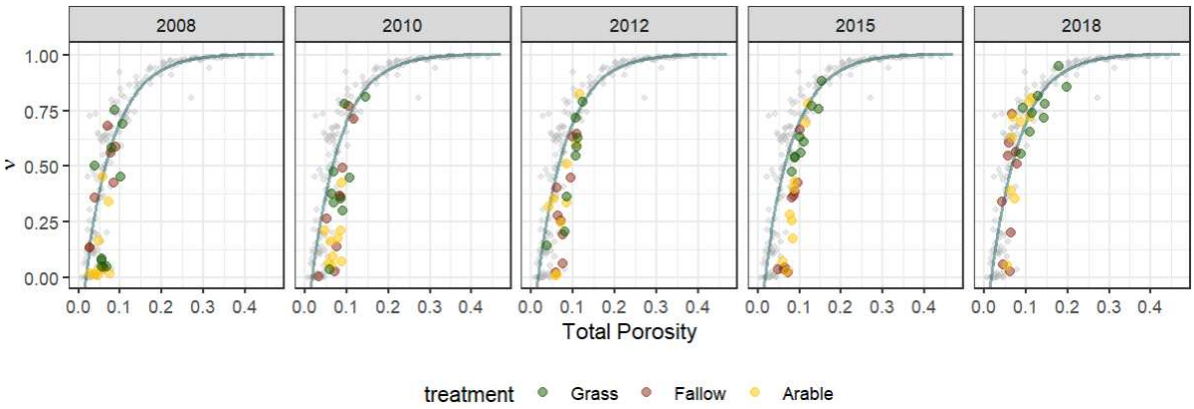


Figure 4. Data suggest complex dynamics following perturbation and that detectable SC takes seven years to establish after intervention on degraded soil. The proportion of connected porosity (v) as a function of total porosity (P_t) in 2-mm sized aggregates scanned at 1.5-µm resolution using X-ray computed tomography for the Highfield reversion experiment. Data points from Fig. 1 are shown in grey, and the best fitting curve from Fig. 1 is shown in green). Soil that was previously bare fallowed for 49 years (orange data points) was re-planted in 2007 with two treatments: permanent grass (green data points) and continuous wheat with annual ploughing (yellow data points). Evidence of departure from the curve observed in the long-term experiments (Fig. 1) persists for seven years following the perturbation. The parameters β and P^* in the relation $v \propto |P_t - P^*|^{\beta}$ are not significantly different between 2015 (n = 27) and 2018 (n = 25), nor are they significantly different from the experiments shown in Fig 2.

The data up to 2012 deviates from significant power-law behaviour, and there is no significant correlation between carbon and P_t. This is consistent with the dynamics during the period up to five years post-establishment being predominantly transient. The deviation is either because the emergence of SC takes at least eight years following disturbance or fluctuations[45] associated with critical slowing down in SC dominate the data when soil is near the tipping point. The gradient of the linear relations between carbon and porosity for 2018 (eleven-years post-perturbation) is not significantly different from the values for the experiments at Broadbalk, Highfield, Longlands and FarmEd (see Fig. 3). The data for 2015 demonstrate power-law behaviour, but with a slope that is significantly different from the other experiments (see Figure 2).

We tested the influence of year (or time since conversion) and management upon *v* in the reversion soils. There was a significant influence of management as either bare fallow, arable or grassland (ANOVA; $F_{2,119} = 13.4$, $p = 6 \cdot 10^{-6}$) and a significant influence of time *post* conversion (ANOVA; $F_{4,119} = 7.2$, $p = 3 \cdot 10^{-5}$), but no significant interaction between the two factors. Effect size, assessed as partial eta-squared (η_p^2), suggested a slightly larger influence of time *post* conversion ($\eta_p^2 = 0.2$) than management ($\eta_p^2 = 0.19$). Benjamini-Hochberg corrected, right-tailed Dunnett contrasts testing whether observed *v* for each management in each year *post* conversion was significantly greater than that of the starting bare fallow soil (2008) identified that only in 2015 and 2018 and under conversion to grassland was *v* increased over the starting *v*.

Therefore, our data provide evidence that condition 4 for SC is met, namely that soil has complex transient dynamics following a perturbation characteristic of proximity to the critical point in SC, which persists for ten years after a change in management.

Sandy Soil Does Not Form a Self-Organised Critical State

In contrast to all other soil types, the data from the Woburn experiment provide no evidence of critical behaviour (Fig 1). The management treatments are similar as for the

Broadbalk Experiment, although they have been running for 85 years instead of 180 years at Broadbalk. Based on the results reported, it is unlikely that the different duration of the experiments is a factor in the lack of critical behaviour because most of the temporal trends in soil properties show evidence of stabilisation[46].

In addition to the lack of evidence of a critical point, there is no significant relation between carbon content and porosity and therefore no evidence for carbon acting as a control variable. There is also a clear deviation of the trend and in the range of data values in the Woburn Experiment compared with that in the data sets for all the other soils. A possible interpretation is that the proportion of particles larger than 50μm (sand) in the soils in the Woburn Experiment is a factor. Particle size and shape influence the nature of percolation and SC in physical systems[47]. In addition to the well-documented interaction between clay particles and organic matter[48], a high sand content may prevent the formation of disconnected pore space because there is an insufficient volume of small particles to fill the voids between grains. If that is the case, then we predict that there will be a rapid transition at a particular sand content in the capacity to form a self-organised critical state.

Discussion and Conclusions

We provide evidence of SC and a tipping point in the soil-microbe ecosystem, and present a general dynamical systems theory for the impact of soil type and land management on soil functioning and organic carbon dynamics.

The presented data provide evidence for a single non-linear relation between connected porosity and total porosity across five soil types and 18 management practices, with a tipping point at a total porosity of 1.7% and power-law behaviour in the vicinity of the tipping point. Time series data show complex transient behaviour close to the tipping point that recovers on decadal timescales following a major perturbation. The exception is the most extreme sandy soil (sand content = 70%). In the latter case, the evidence points to the soil being in a different material state to the soils with a lower sand content. For the remaining soils and management practices, the data are consistent with a linear relation between total porosity and soil organic carbon content, with a common slope. Taken together with the predictions of a simple model for the interaction between microbial activity and soil structural genesis, the evidence is consistent with there being a universal self-organised critical state for soil with carbon input as the control variable.

This conclusion suggests that the soil ecosystem naturally evolves to the edge of instability (close to the critical/tipping point) through purely endogenous processes. This state enables the soil ecosystem to adapt quickly to changes in energy (organic carbon) input rates to maintain a store of energy. It also helps ensure that soil does not reach the tipping point, even under the most extreme mismanagement of carbon inputs. Soils that are further from the tipping point have higher porosity and a greater proportion of that pore space is connected. Our previous work shows that these soils have more efficient microbial metabolism, they store more water and nutrients, and the rate of movement of water and nutrients towards roots will be greater[20,44]. Conversely, soils that are closer to the tipping point store less water and nutrients, metabolism is slower and less efficient, and transport rates are significantly reduced[20]. Management practises that reduce net carbon inputs, resulting in less stored carbon, push soils closer to the tipping point.

The approach we have adopted here allows us to explore potential consequences of a complex dynamical state on resilience and functioning of the soil ecosystem. In particular, we show evidence of non-equilibrium transient behaviour following a major perturbation (Fig. 4). A full exploration requires additional data from long-term experiments, but the data presented here allow us to propose several hypotheses.

The data from the Highfield Reversion experiment (Fig. 4) show that it requires at least 10 years following a major perturbation for the soils to return to the same state as the unperturbed soils at Highfield. Total porosity recovers first, followed by the connected porosity. A significant power-law relation between connected porosity and porosity appears at 2015, but it is significantly different from that shared between the 2018 treatment and the other soils studied. However, even after 10 years, the grassland reversion treatments have not recovered the porosities of their parent treatments. Previous work on the Rothamsted Long-Term Experiments show that soil is still recovering (measured by carbon content) from the point of establishing the experimental treatments in 1843, albeit with most of the recovery in the first few decades[49]. While the linear relationship between soil organic carbon and porosity has the same slope across the Highfield, Broadbalk, FarmED, Longlands, and Highfield Reversion, the normalisation (height) of the linear relations is markedly different. Notably, the shorter experiments (Longlands, FarmED, Highfield Reversion) have lower porosity for a given carbon content than the longer-term experiments (Broadbalk and Highfield). Broadbalk has the highest (est. 1843), followed by Highfield (est. 1948), followed by the others (est. circa 2010). We can therefore hypothesise that the distance of a soil from the tipping point depends on both carbon inputs (as affected e.g. by management) and time, and that the 'memory' of perturbation remains in the signature of the dynamical state of soil for decades.

If we accept that a basis of soil health is a dynamical state that enables soil to maintain biological and physical functioning in the face of perturbations in energy inputs and disturbance, then the potential existence of a universal self-organised critical state is significant. Soils that are closer to the tipping point could be regarded as being in poorer health because they take longer to recover due to critical slowing down[45], store less water and nutrients, transport water and nutrients more slowly, and have lower and less efficient microbial metabolism than those that are farther away. Importantly, while recovery is fast due to the characteristics of SC, it takes decades to recover full health.

The soil in the Woburn experiment did not show evidence of SC, and as such is in a different material state. It is not clear that the same definition of soil health would apply to this sandy soil. More data that fills the gap in sand content between Woburn and the rest of the soils used in this study is needed to know if this is a general property of sandy soils, and whether the loss of the capacity for SC is abrupt or gradual.

Our results indicate that the soil processes linked to the planetary boundaries[50] will likely deteriorate disproportionately as the tipping point is approached but that a tipping point will likely be avoided. The caveat to that is where soil degradation leads to the loss of fine particles (e.g. desertification[2]), potentially resulting in a change of the material properties of soil due to the loss of the self-organised critical state. The consequences for the planetary boundaries would be profound, and if the generality of self-organised critical behaviour is confirmed, this has important policy implications.

Acknowledgements.

This research was supported by the United Kingdom's Biotechnology and Biological Science Research Council (BBSRC)-funded *Soil to Nutrition* (BBS/E/C/000I0310) and *Growing Health* (BB/X010953/1; BBS/E/RH/230003B) strategic programs. Access to the Highfield, Broadbalk and Woburn experiments is supported by the Lawes Agricultural Trust and the National Bioscience Research Infrastructure funded by BBSRC (2012-2017, BBS/E/C/00005189; 2017-2022, BBS/E/C/000J0300; 2023-2028 BBS/E/RH/23NB0007).

Contributions.

JWC, ALN, and IMY conceived the study, and JWC and ALN contributed equally to the design. ABL and SJM acquired the CT data, and ABL analysed this data, while ALN did the analysis presented in this paper's Figures. JWC developed the mathematical model behind equation 1 with contributions from CH. JWC, ALN, CH, XXZ, WR, and SK contributed to the interpretation of data. JWC wrote the manuscript with contributions from all the authors.

References

1. Winowiecki, L. A. *et al.* Multistakeholder Engagement to Scale Soil Health Globally: The Coalition of Action 4 Soil Health. *Eur. J. Soil Sci.* **76**, e70128 (2025).
2. Intergovernmental Panel on Climate Change. *Climate Change and Land: IPCC Special Report on Climate Change, Desertification, Land Degradation, Sustainable Land Management, Food Security, and Greenhouse Gas Fluxes in Terrestrial Ecosystems*. (Cambridge University Press, 2022). doi:10.1017/9781009157988.
3. Timmis, K. & Ramos, J. L. The soil crisis: the need to treat as a global health problem and the pivotal role of microbes in prophylaxis and therapy. *Microb. Biotechnol.* **14**, 769–797 (2021).
4. Lehmann, J., Bossio, D. A., Kögel-Knabner, I. & Rillig, M. C. The concept and future prospects of soil health. *Nat. Rev. Earth Environ.* **1**, 544–553 (2020).
5. Sadiq, F. K. *et al.* Conservation Agriculture for Sustainable Soil Health Management: A Review of Impacts, Benefits and Future Directions. *Soil Syst.* **9**, 103 (2025).

6. Khangura, R., Ferris, D., Wagg, C. & Bowyer, J. Regenerative Agriculture—A Literature Review on the Practices and Mechanisms Used to Improve Soil Health. *Sustainability* **15**, 2338 (2023).
7. Guo, M. Soil Health Assessment and Management: Recent Development in Science and Practices. *Soil Syst.* **5**, 61 (2021).
8. Țopa, D.-C., Căpșună, S., Calistru, A.-E. & Ailincăi, C. Sustainable Practices for Enhancing Soil Health and Crop Quality in Modern Agriculture: A Review. *Agriculture* **15**, 998 (2025).
9. Hughes, H. M. *et al.* Towards a farmer-feasible soil health assessment that is globally applicable. *J. Environ. Manage.* **345**, 118582 (2023).
10. Smith, P. *et al.* How to measure, report and verify soil carbon change to realize the potential of soil carbon sequestration for atmospheric greenhouse gas removal. *Glob. Change Biol.* **26**, 219–241 (2020).
11. Shi, Z., Crowell, S., Luo, Y. & Moore, B. Model structures amplify uncertainty in predicted soil carbon responses to climate change. *Nat. Commun.* **9**, 2171 (2018).
12. Yang, J., Li, A., Yang, Y., Li, G. & Zhang, F. Soil organic carbon stability under natural and anthropogenic-induced perturbations. *Earth-Sci. Rev.* **205**, 103199 (2020).
13. Ma, Y. *et al.* Global crop production increase by soil organic carbon. *Nat. Geosci.* **16**, 1159–1165 (2023).
14. Lal, R. Nature-based solutions of soil management and agriculture. *J. Soil Water Conserv.* **77**, 23A-29A (2022).
15. Paustian, K., Larson, E., Kent, J., Marx, E. & Swan, A. Soil C Sequestration as a Biological Negative Emission Strategy. *Front. Clim.* **1**, (2019).
16. Vogel, H.-J. *et al.* A systemic approach for modeling soil functions. *SOIL* **4**, 83–92 (2018).

17. Harris, J. A., Evans, D. L. & Mooney, S. J. A new theory for soil health. *Eur. J. Soil Sci.* **73**, e13292 (2022).

18. Hassan-Dalléac, S., Guiga, W. & Suau-Pernet, A. Soil microbes are the tiny bioengineers running Earth's underground factory. *Commun. Earth Environ.* **7**, 403 (2026).

19. Hartmann, M. & Six, J. Soil structure and microbiome functions in agroecosystems. *Nat. Rev. Earth Environ.* 1–15 (2022) doi:10.1038/s43017-022-00366-w.

20. Neal, A. L. *et al.* Soil as an extended composite phenotype of the microbial metagenome. *Sci. Rep.* **10**, 10649 (2020).

21. Bordoloi, S., Ni, J. & Ng, C. W. W. Soil desiccation cracking and its characterization in vegetated soil: A perspective review. *Sci. Total Environ.* **729**, 138760 (2020).

22. Pachepsky, Y. & Hill, R. L. Scale and scaling in soils. *Geoderma* **287**, 4–30 (2017).

23. Young, I. M. & Crawford, J. W. Interactions and Self-Organization in the Soil-Microbe Complex. *Science* **304**, 1634–1637 (2004).

24. Crawford, J. W., Harris, J. A., Ritz, K. & Young, I. M. Towards an evolutionary ecology of life in soil. *Trends Ecol. Evol.* **20**, 81–87 (2005).

25. Crawford, J. W. *et al.* Microbial diversity affects self-organization of the soil–microbe system with consequences for function. *J. R. Soc. Interface* **9**, 1302–1310 (2011).

26. Feeney, D. S. *et al.* Three-dimensional microorganization of the soil-root-microbe system. *Microb. Ecol.* **52**, 151–158 (2006).

27. Young, I. M., Crawford, J. W., Nunan, N., Otten, W. & Spiers, A. Microbial Distribution in Soils: Physics and Scaling. in *Advances in Agronomy, Vol 100* (ed. Sparks, D. L.) vol. 100 81–121 (Elsevier Academic Press Inc, San Diego, 2008).

28. Marković, D. & Gros, C. Power laws and self-organized criticality in theory and nature. *Phys. Rep.* **536**, 41–74 (2014).

29. Bak, P., Tang, C. & Wiesenfeld, K. Self-organized criticality. *Phys. Rev. A* **38**, 364–374 (1988).

30. Rivera, A. L., Toledo-Roy, J. C. & Frank, A. Symmetry and Signs of Self-Organized Criticality in Living Organisms. *J. Phys. Conf. Ser.* **1612**, 012024 (2020).

31. Stauffer, D. Scaling theory of percolation clusters. *Phys. Rep.* **54**, 1–74 (1979).

32. Soto-Gómez, D. *et al.* Percolation theory applied to soil tomography. *Geoderma* **357**, 113959 (2020).

33. Jarvis, N., Larsbo, M. & Koestel, J. Connectivity and percolation of structural pore networks in a cultivated silt loam soil quantified by X-ray tomography. *Geoderma* **287**, 71–79 (2017).

34. Scheffer, M. *et al.* Early-warning signals for critical transitions. *Nature* **461**, 53–59 (2009).

35. Neal, A. L. *et al.* Arable soil nitrogen dynamics reflect organic inputs via the extended composite phenotype. *Nat. Food* **4**, 51–60 (2023).

36. Hirsch, P. R. *et al.* Soil resilience and recovery: rapid community responses to management changes. *Plant Soil* **412**, 283–297 (2017).

37. Johnston, A. E., Poulton, P. R. & Coleman, K. Chapter 1 Soil Organic Matter. in *Advances in Agronomy* vol. 101 1–57 (Elsevier, 2009).

38. Hawkins, J., Griffith, B., Sint, H. & Harris, P. The North Wyke Farm Platform: Design, Establishment and Development. https://doi.org/10.23637/ROTHAMSTED.98Y1X (2023) doi:10.23637/ROTHAMSTED.98Y1X.

39. Xu, X., Wang, J., Lv, J.-P. & Deng, Y. Simultaneous analysis of three-dimensional percolation models. *Front. Phys.* **9**, 113–119 (2014).

40. Harter, T. Finite-size scaling analysis of percolation in three-dimensional correlated binary Markov chain random fields. *Phys. Rev. E* **72**, 026120 (2005).

41. Johannes, A. *et al.* Optimal organic carbon values for soil structure quality of arable soils. Does clay content matter? *Geoderma* **302**, 14–21 (2017).

42. Fukumasu, J., Jarvis, N., Koestel, J., Kätterer, T. & Larsbo, M. Relations between soil organic carbon content and the pore size distribution for an arable topsoil with large variations in soil properties. *Eur. J. Soil Sci.* **73**, e13212 (2022).

43. Rappoldt, C. & Crawford, J. W. The distribution of anoxic volume in a fractal model of soil. *Geoderma* **88**, 329–347 (1999).

44. Zhang, X. *et al.* Relationship between soil carbon sequestration and the ability of soil aggregates to transport dissolved oxygen. *Geoderma* **403**, 115370 (2021).

45. Network resilience - ScienceDirect. https://www.sciencedirect.com/science/article/pii/S0370157322001211?via%3Dihub.

46. The Long Term Experiments. *Rothamsted Research* https://www.rothamsted.ac.uk/long-term-experiments.

47. Lin, J., Chen, H. & Liu, L. Impact of polydispersity of particle shape and size on percolation threshold of 3D particulate media composed of penetrable superellipsoids. *Powder Technol.* **360**, 944–955 (2020).

48. Poeplau, C. & Don, A. A simple soil organic carbon level metric beyond the organic carbon-to-clay ratio. *Soil Use Manag.* **n/a**,.

49. Powlson, D. S. *et al.* The potential to increase soil carbon stocks through reduced tillage or organic material additions in England and Wales: A case study. *Agric. Ecosyst. Environ.* **146**, 23–33 (2012).

50. Kopittke, P. M. *et al.* The role of soil in defining planetary boundaries and the safe operating space for humanity. *Environ. Int.* **146**, 106245 (2021).

51. Hogan, D. THE SOILS OF NORTH WYKE AND ROWDEN.

52. The <fc>N</fc>orth <fc>W</fc>yke <fc>F</fc>arm <fc>P</fc>latform: effect of temperate grassland farming systems on soil moisture contents, runoff and associated water quality dynamics - Orr - 2016 - European Journal of Soil Science - Wiley Online Library. https://bsssjournals.onlinelibrary.wiley.com/doi/10.1111/ejss.12350.

53. Hawkins, J., Beaumont, D., Sint, H. & Harris, P. *The North Wyke Farm Platform: Field Survey Data*. https://repository.rothamsted.ac.uk/id/eprint/32697/ (2023) doi:10.23637/rothamsted.98y51.

54. Hawkins, J., Griffith, B., Sint, H. & Harris, P. The North Wyke Farm Platform: Design, Establishment and Development. https://doi.org/10.23637/ROTHAMSTED.98Y1X (2023) doi:10.23637/ROTHAMSTED.98Y1X.

55. Livestock Performance for Sheep and Cattle Grazing Lowland Permanent Pasture: Benchmarking Potential of Forage-Based Systems. https://www.mdpi.com/2073-4395/9/2/101.

56. Schneider, C. A., Rasband, W. S. & Eliceiri, K. W. NIH Image to ImageJ: 25 years of image analysis. *Nat. Methods* **9**, 671–675 (2012).

57. Vogel, H. J. & Kretzschmar, A. Topological characterization of pore space in soil — sample preparation and digital image-processing. *Geoderma* **73**, 23–38 (1996).

58. Vogel, H.-J., Weller, U. & Schlüter, S. Quantification of soil structure based on Minkowski functions. *Comput. Geosci.* **36**, 1236–1245 (2010).

59. Wang, M. *et al.* Global soil profiles indicate depth-dependent soil carbon losses under a warmer climate. *Nat. Commun.* **13**, 5514 (2022).

60. Bacq-Labreuil, A. *et al.* Effects of cropping systems upon the three-dimensional architecture of soil systems are modulated by texture. *Geoderma* **332**, 73–83 (2018).

61. Rothamsted Research. Broadbalk soil organic carbon content 1843-2015. 73 KB, 35 KB Electronic Rothamsted Archive, Rothamsted Research https://doi.org/10.23637/KEYREFOABKSOC-02 (2021).

62. R Core Team. (2025) R A Language and Environment for Statistical Computing. R Foundation for Statistical Computing. - References - Scientific Research Publishing. https://www.scirp.org/reference/referencespapers?referenceid=3967248.

63. Warton, D. I., Wright, I. J., Falster, D. S. & Westoby, M. Bivariate line-fitting methods for allometry. *Biol. Rev.* **81**, 259–291 (2006).

64. Krzanowski, W. J. Principal Component Analysis in the Presence of Group Structure. *J. R. Stat. Soc. Ser. C Appl. Stat.* **33**, 164–168 (1984).

Supplementary material

Sampling and Imaging Methods

All data used in our analysis was collected from a series of long-term field experiments operated and managed by Rothamsted Research in southeast England.

Highfield Ley-Arable experiment (51° 48' 10.0" N, 0° 21' 57.7" W, 130 m above sea level,) is managed by Rothamsted Research in southeast England. Set on a silty-clay loam textured soil developed on clay-with-flints over Eocene London Clay (Batcome series) and classified as a Chromic Luvisol by FAO criteria The soil has a silty-clay loam texture. We studied soils under three contrasting managements. The first was a grassland, present since at least 1838. Grassland plots are maintained as a managed mixed sward of fescue (*Festuca pratensis* L.), Timothy grass (*Phleum pratense* L.) and white clover (*Trifolium repens* L.). Fertilizers (250 kg-K ha^{-1} as K_2SO_4 and 65 kg-P ha^{-1} as triple superphosphate [$Ca(H_2PO_4)2{\cdot}H_2O$]) are added every three years and hay mowed and removed annually. The second treatment was a set of arable plots established in 1949 and managed as a continuous wheat rotation (winter wheat, *Triticum aestivum* L., c.v. “Hereward”) and planted with seeds coated with the triazole fungicides prothioconazole ($C_{14}H_{15}Cl_2N_3OS$) and tebuconazole ($C_{16}H_{22}ClN_3O$, Redigo Deter, Bayer CropScience, UK). Arable plots are fertilized each year to provide 220 kg-N ha^{-1} $year^{-1}$ as ammonium nitrate (NH_4NO_3) and 250 kg-K ha^{-1} and 65 kg-P ha^{-1} every three years. The third treatment was plots managed as bare fallow, established in 1959. These plots are maintained with regular tillage or rotavation at least four times per year to prevent any plant growth. Arable and bare-fallow plots are tilled to a depth of approximately 30 cm. The replication of treatments was a minimum of nine aggregates scanned from cores collected from three replicate plots of each treatment (total, 32 aggregates).

Broadbalk Winter Wheat long-term experiment (51° 48' 34.1" N, 0° 22' 22.8" W, 130 m above sea level, http://www.era.rothamsted.ac.uk/experiment/rbk1) managed by Rothamsted Research in southeast England. Set on a similar soil texture to the near-by Highfield experiment, this field experiment was established in 1843 and is managed under

continuous wheat rotations (winter wheat, *T. aestivum* L., most recently using Crusoe [2013-2018] and Zyatt [since 2018] cultivars). As with the Highfield arable plots, seed is coated with dual fungicides. The soils provided a range of soil organic carbon stocks. We sampled soil from several contrasting fertility managements including receiving 35 Mg ha^{-1} yr^{-1} composted farmyard manure from cattle; 144 kg-N ha^{-1} yr^{-1} together with 90 kg-K ha^{-1} yr^{-1}, 35 kg-P ha^{-1} yr^{-1}, and 12 kg-Mg ha^{-1} yr^{-1} as $MgSO_4$; 192 kg-N ha^{-1} yr^{-1} together with 90 kg-K ha^{-1} yr^{-1} and 12 kg-Mg ha^{-1} yr^{-1} (i.e., lacking phosphorus fertilisation); 90 kg-K ha^{-1} yr^{-1}, 35 kg-P ha^{-1} yr^{-1} and 12 kg-Mg ha^{-1} yr^{-1} (i.e., lacking nitrogen fertilisation); and soil which had never received any fertilisation for the duration of the experiment. The replication of treatments was a minimum of seven aggregates scanned from three pseudo-replicate cores from treatment plots collected from Section 1 of the field experiment (total, 42 aggregates). Highfield Conversion experiment (51° 48' 15.5" N, 0° 21' 45.7" W, 130 m above sea level). In October 2008, plots of soil managed as bare fallow since 1959 (described above) were converted to arable or grassland managements. Management of the plots converted to grassland and arable is as described above for the permanent managements. Plots have been sampled annually in October—except in 2018 when the plots were sampled in June—using 10-cm. depth by 3-cm. diameter cores. Following sampling, soil was air-dried and sieved at 2 mm before being archived at room temperature. Aggregates (<2 mm diameter) from continuous bare-fallow (bare-fallow), bare-fallow converted to arable (arable) and bare-fallow converted to grassland (grassland) were selected randomly from samples collected in 2008, 2010, 2012, 2015 and 2018, representing 0, 2-, 4-, 7- and 10-years post-conversion. The replication of treatments was a total of nine scanned aggregates (<2 mm) per year and per treatment selected from three independent plots per treatment and three aggregates (<2 mm) per plot (i.e., three replicates per plot) to be X-ray CT scanned (total, 135 aggregates).

For the field experiments set on Highfield and Broadbalk, the climate metrics measured nearby (51° 48' 24.8" N, 0° 21' 36.5" W) between 1991-2020 were mean annual rainfall 764 mm (range of average monthly totals, 47.1 – 81.3 mm), average annual minimum air temperature 6.4 °C (monthly average range, 1.6 – 12.3 °C), mean soil temperature at a depth of 30 cm. under grass 10.9 °C (monthly average range, 5.1 – 17.2 °C), mean annual total solar radiation 3,607 MJ m^{-2} (average monthly total range 61.7 – 548.0 MJ m^{-2}).

Woburn Organic Manuring experiment (51° 59' 59.3" N, 0° 36' 57.7" W, 100 m above sea level, https://doi.org/10.23637/wrn3-cropping1938-2020-02). Established in 1964, this field experiment is set on a well-draining, sandy loam soil of the Cottenham Series, classified as a Cambric Arenosol (FAO). We sampled soil from each of four sub-plots of three contrasting treatments: grass-clover herbal leys, arable soil amended with 25 Mg ha^{-1} composted farmyard manure, and arable soil receiving 200 kg-N ha^{-1} (as ammonium nitrate). The arable plots are managed as a rotation of rye, barley and wheat and the amount of nitrogen fertiliser input varies between years as follows: rye receives 120 kg-N ha^{-1}; barley receives 140 kg-N ha^{-1}; and maize and wheat receive 200 kg-N ha^{-1}. All plots were sampled when under wheat to be consistent with the Highfield and Broadbalk treatments. For the Woburn site, climate metrics recorded between 1991 and 2020 at a nearby weather station (52° 0' 52.2" N, 0° 35' 46.3" W) were mean total annual rainfall 671 mm (range of average monthly totals, 41.7 – 74.0 mm), mean annual minimum air temperature 6.1 °C (monthly average range, 1.4 – 11.9 °C), mean soil temperature at a depth of 30 cm. under grass 11.1 °C (monthly average range, 5.1 – 17.9 °C), and mean annual total solar radiation 3,477 MJ m^{-2} (average monthly total range 58.0 – 534.1 MJ m^{-2}). Air and soil daily temperatures for the periods 27th March – 5th July 2007 and 16th June – 26th July 2009 have been omitted from the estimates of means due to technical issues. The replication of treatments was a minimum of eleven aggregates scanned from one core collected from the three replicate treatment plots (total, 37 aggregates).

The fields Longlands North, Longlands South and Longlands East are situated on the Rothamsted Research North Wyke Farm Platform (NWFP), a farm-scale experiment situated in southwest England (50° 46’ 12” N, 3° 54’ 05” W, 120–190 a.m. above sea level). The fields share a common soil type (Hallsworth series, Dystric Gleysol) having a slightly stony clay loam topsoil (approximately 36% clay) overlying a mottled stony clay (approximately 60% clay), derived from underlying Carboniferous culm rocks[51]. From 1982 to 2019, the average annual precipitation was 1031 mm (range, 705–1361 mm) and the average minimum and maximum daily air temperatures were 6.8 and 13.5 °C, respectively.
The 63-ha Farm Platform site was established in 2010 and is comprised of fifteen hydrologically isolated (sub-) catchments distributed between three 21-ha small farms

(farmlets), each with five (sub-) catchments[52]. The platform monitors soil, livestock and silage performance together with records of farm management events routinely[53,54]. These data are coupled with primary collections of weather variables, soil moisture, water flux and chemistry, and greenhouse gases. Datasets are freely available from the NWFP Data Portal (https://nwfp.rothamsted.ac.uk/), including those used in this study. Up until July 2013 the three fields were managed as permanent pastures of predominantly perennial ryegrass (*Lolium perenne* L.) with some self-sown grasses, legumes and non-legume forbs, and had similar livestock performance[55]. After 2013, Longlands South and Longlands North were managed as improved pastures of either a high-sugar perennial ryegrass (*L. perenne* cv. AberMagic) fertilised with ammonium nitrate, or a combination of white clover (*Trifolium repens* L. cv. AberHerald, approximately 30% cover) and high-sugar perennial ryegrass without nitrogen fertilisation respectively. To maintain the clover population, Longlands North was reseeded every four years, requiring tillage. Until 2019, all fields received same rates of P and K fertilizers and farmyard manure. In 2019, Longlands East was ploughed and converted to arable management (at the time of sampling, winter wheat, *Triticum aestivum* L. cv. Crusoe). It has been ploughed annually since and it has not received any organic amendment. The replication of treatments was a minimum of eleven aggregates scanned from triplicate cores collected from each field (total, 68 aggregates).

Soils were also studied from FarmED, Shipton-under-Wychwood (51° 52′ 13″ N, 1° 34′ 52″ W, 113 m above sea level), a demonstration farm in the south of England with 1991-2024 mean monthly precipitation of 63.2 mm and mean monthly temperature of 6.3 °C. Soils are predominantly free-draining shallow lime-rich clay loams and over chalk or limestone derived from Middle Jurassic oolitic limestone. Since autumn 2014, eight strips of approximately 0.8 ha each have been managed in a staggered eight-year rotation (four years of multi-species herbal ley followed by four years of cereals), with each strip at a different rotational stage in any given year. The herbal leys comprised five grass species, seven legume species, and six herb species, grazed by sheep and terminated by inversion tillage. Two additional plots, a 0.96-ha continuous no-till cereal plot (no-till annual) and an approximately 3-ha long-term (LT) organic permanent pasture (perennial-LT), served as examples of annual cereal cropping in the absence of herbal leys and long-term perennial management. Prior to 2014, all rotation and no-till plots were managed as tilled, inorganically

fertilised continuous arable. Tillage in the continuous no-till cereal plot continued until 2020, after which the plot was managed as no-till. The experimental layout followed a time-for-space substitution structure, in which spatially discrete plots represented different stages of an eight-year rotation and contrasting long-term management states. We collected aggregates from cores collected from the permanent pasture, the no-tilled permanent arable, a four-year-old herbal ley, and an arable plot within the cereal rotation which had been under a four-year-old herbal ley terminated by inversion tillage and power harrow six weeks before sampling. The replication of treatments was a minimum of five aggregates scanned from triplicate cores collected from each field (total, 28 aggregates).

X-ray Computed Tomography of Soil Aggregates. We generated X-ray Computed Tomography (CT) images at 1.5-µm resolution and scales relevant to microbes (10^0–10^2 µm), requiring imaging of soil aggregates having a diameter of no greater than 2 mm. Soil aggregates were recovered from sampled soils following air-drying overnight. The soil was passed through 4-, 2- and 0.71-mm mesh size sieves while being subjected to horizontal shaking for 3 min at 300 rotations min^{-1}. Aggregates were selected at random from between the 2- and 0.71-mm sieves and conserved in sealed containers in the dark at room temperature until they were scanned. These were scanned using a Phoenix Nanotom X-ray Computed Tomography system (GE Measurement and Control solution, Wunstorf, Germany) set at 90 kV, a current of 65 µA and at a base resolution of 1.51 µm (voxel volume resolution = 3.4 $µm^3$). Projection images were taken at 500 ms period using an averaging of 3 images and skip of 2. Typical scan times per aggregate were approximately 70 minutes.

Analysis of Tomographic Images. Initial image analysis was performed using ImageJ[56]. Cubic regions of interest (ROI) for aggregates were not possible because of their variable geometry, so the largest ROI accommodated by all aggregates (981 × 725 × 604 µm) was chosen. The coordinates of these regions were adapted for each image volume and sequence. Image pre-processing consisted of: (i) cropping to the ROI; (ii) enhancing the contrast/brightness to 0.35%; (iii) application of a 2-pixel radius median filter; (iv) converting

the image format to 8-bit; (v) saving the new image volume. Stones were segmented from the ROI volume in VG StudioMax® 2.2 using the surface determination tool.

Segmentation of grey-scale images to generate binary images was performed using the bin bi-level threshold approach[57] using the open source software QuantIm (http://www.quantim.ufz.de). Each image within the image sequence was assigned a single threshold value. To determine the prescribed initial threshold values (T_1 and T_2), minimum cross-threshold entropy was applied to twenty images selected at random within the image sequence in ImageJ. Threshold values (T_1 and T_2) were attributed depending on extremes values obtained for these twenty images. Porosity and pore connectivity were determined according to Vogel et al.[58] Total porosity (P_t) refers to the percentage of pores >1.8 µm determined from segmented images. Pore connectivity (P_c) was defined as the pore space through which an uninterrupted path exists between the upper and lower borders of the ROI.

Soil Organic Carbon Stocks. Stocks of organic carbon measured by dry combustion and element specific detection associated with the long-term experiments are estimated routinely. Stocks for the individual experiments have been reported elsewhere[20,35,59,60,61].

Modelling Soil Respiration Close to the Tipping Point

As stated in the main body of the paper, we start with the assumption that microbial respiration is a zeroth order function of the oxygen concentration (i.e. the respiration per unit volume is Q for all $C > 0$, and is zero for $C = 0$). The equation describing the distribution of oxygen in soil can then be written:

$$\frac{\partial C}{\partial t} = \nabla^2 DC - Q \ , \qquad (1)$$

where C is the oxygen concentration, D is the oxygen diffusion coefficient, and Q is the potential respiration rate per unit volume. Assuming planar geometry, this can be written in non-dimensional form by making the following substitutions:

$$\gamma = \frac{C}{C_a}; \quad \tau = \frac{t}{t_0}; \quad \chi = \frac{x}{L} \ ; \ \kappa = \frac{Q t_0}{C_a} \ ; \ t_0 = \frac{L^2}{D}$$

where C_a is the atmospheric oxygen concentration, L is the depth to which oxygen penetrates the soil profile, and $t_0 = L^2/D$. The non-dimensional form of equation 1 is then,

$$\frac{\partial \gamma}{\partial \tau} = \nabla^2 D\gamma - \kappa\,, \qquad (2)$$

This has the following boundary conditions at the steady state,

$$\chi = 0 \;\Rightarrow\; \gamma = 1$$

$$\chi = 1 \;\Rightarrow\; \gamma = 0 \text{ and } \frac{\partial \gamma}{\partial x} = 0$$

Leading to the solution,

$$\gamma(\chi) = \begin{cases} (1-\chi)^2, & \chi \leq 1 \\ 0, & \chi > 1, \end{cases} \qquad (3)$$

and

$$\kappa = 2 \qquad (4)$$

Returning to the dimensional form and using equation 4, the length scale, L, can be expressed in the following form,

$$L = \sqrt{\frac{2DC_a}{Q}} \qquad (5)$$

Because we have assumed respiration is a zeroth order function of oxygen, the respiration per unit soil surface area, r_n, is given by the product QL. Therefore, using equation 5, we can express the soil respiration rate as,

$$r_n = \sqrt{2QDC_a} \qquad (6)$$

To explore the consequences of self-organised critical behaviour, we first assume that the diffusion rate is a power-law function of porosity[44,20],

$$D = D_0 \left(\frac{\rho}{\rho_0}\right)^{\alpha}, \qquad (7)$$

where ρ is the porosity, ρ_0 is a constant, and α is the power-law exponent. If we then make the assumption that the porosity is a power-law function of potential respiration rate, $\rho \propto Q^{\beta}$, we can rewrite equation 7 in the form,

$$D = D_0 \left(\frac{Q}{Q_0}\right)^{k}, \qquad (8)$$

Where Q_0 is a constant, and k is a constant that measures the strength of the positive feedback between carbon metabolism and oxygen transport rate. Using this equation to substitute for D in equation 6 yields an expression for respiration as a function of Q, which we denote as r_k, of the form,

$$r_k = \sqrt{\frac{2DC_a}{{Q_0}^k}}\, Q^{(1+k)/2} \qquad (9)$$

In the steady state, the value of Q will correspond to the equilibrium soil carbon content, and equation 9 can be rearranged to express Q in terms of the respiration rate,

$$\frac{Q}{Q_0} = \left(\frac{r}{r_o}\right)^{\frac{2}{1+k}} \qquad (10)$$

where,

$$r_0 = \frac{2DC_a}{{Q_0}^{(k-1)/2}}$$

In the steady state, the rate of loss of carbon from the system will equal the rate of input. Therefore, if we denote the carbon flux into the soil as f_c, then we can write,

$$f_c = \alpha r$$

where α is a constant of proportionality. Then, using equation 10, the relation between the equilibrium soil carbon content and the carbon input flux can be expressed as,

$$\frac{Q}{Q_0} = \left(\frac{f}{f_o}\right)^{\frac{2}{1+k}} \qquad (11)$$

where $f_0 = \alpha r_0$.

In the absence of coupling between structure and microbial activity, $k = 0$, and the power-law exponent in equation 11 is equal to 2. As we increase the strength of the coupling, k progressively increases, and this has contrasting consequences for the equilibrium soil carbon content when the input flux is low ($f \ll f_0$) compared to high input flux ($f \gg f_0$). In the former case, the equilibrium soil carbon content is higher in the presence of coupling between structure and microbial activity and increases monotonically with k for all $k > 0$. In the latter case, the equilibrium carbon content is lower and decreases monotonically with k for all $k > 0$. If we associate the coupling of microbial activity and structure with the emergence of SC, then we see that the SC modelled in this way maintains soil carbon levels within a narrower range of values in an environment where carbon inputs fluctuate. This

effect is enhanced when the feedback between structure and microbial metabolism is stronger i.e. for higher values of k.

Statistical Analysis.

All statistical analysis was performed in R version 4.5.3[62].

Relationship between connected porosity against total porosity. The relationship between total porosity (P_t) and the connectivity parameter ν in was described with a von Bertalanffy growth function:

$$\nu = \nu_\infty(1-\exp(-K(P_t-t_0)))$$

where ν_∞ represents the upper limit of pore connectivity (i.e., 1), P_t represents total porosity, and t_0 represents the theoretical total porosity when ν equals zero. The model was fitted by nonlinear least squares using the *nlstools* package version 2.1-0. Starting values were derived from a custom self-starting routine. L_∞ was initialised as the maximum observed ν, t_0 as the minimum observed P_t, and K from the median point of the data by rearranging the model equation,

$$K = -\ln[(L_\infty - \nu_med)/L_\infty] / (P_t_med - t_0).$$

Parameter estimates were reported with their standard errors, *t*-values and probabilities. Overall fit was assessed with the residual standard error, $RSE = \sqrt{[SSE/(n - p)]}$, where *n* is the number of observations and p the number of parameters. A *pseudo*-R^2 was calculated as $1 - SSE/SST$, where SSE and SST are the residual and total sums of squares. The fitted curve and its 95% confidence band were evaluated at each unique observed value of Pt, with no interpolation between points. The standard error of the fitted value at each Pt was obtained by the delta method, $SE = \sqrt{(g^T V g)}$, where g is the gradient of the model with respect to (L_∞, K, t_0) and **V** is the parameter variance–covariance matrix from the fit. The confidence limits were the fitted value ± 1.96 × SE.

The relationship between $\log(P_t - P^*)$ and $\log(\nu)$ was described by major axis (MA) regression.

Tests of individual slopes. For each site, the null hypothesis that the MA slope equals zero was tested following Warton et al.[63]. For a slope of zero this reduces to testing r = 0, using $t = rv[(n - 2)/(1 - r^2)]$ on n − 2 degrees of freedom, with a two-sided probability.

Test for a common slope across sites. The hypothesis that all sites share one MA slope was tested with an inverse-variance weighted Wald-type statistic, $W = \Sigma w_i(b_i - \bar{b}_w)^2$. The weights were $w_i = 1/\mathrm{Var}(b_i)$, with $\mathrm{Var}(b_i) \approx b_i^2(1 - r_i^2)/(n_i - 2)$, and $\bar{b}_w$ is the precision-weighted mean slope. Significance was assessed by permutation: site labels were randomly reassigned across the pooled observations, *W* was recalculated for each permutation, and the probability was the proportion of permuted *W* values greater than or equal to the observed value. The random seed was fixed at 42.

Pairwise comparisons. Where appropriate, sites were compared using the Bartlett-corrected likelihood ratio test for equal MA slopes (Warton *et al*.[63], Appendix D). For each pair, the common slope was estimated by solving the maximum-likelihood score equation numerically with uniroot, starting from the pooled slope of Krzanowski[64]. If the root-finder failed, the pooled slope was used. The test statistic was

$$T = -\Sigma(n_i - 2.5)\cdot\ln(1 - r_{rf,i}^2)$$

where $r_{rf,i}$ is the correlation between residual and fitted axis scores of site *i* under the common slope. *T* was compared with a χ^2 distribution with one degree of freedom. The raw probabilities were adjusted using the Benjamini–Hochberg method to control false discovery rate. Confidence intervals for each site's slope were obtained by the percentile bootstrap, resampling (*x*, *y*) pairs with replacement 1,999 times and taking the 2.5th and 97.5th percentiles. The bootstrap standard error was approximated as the interval width divided by 3.92. Bootstrap MA fit lines were also computed at 200 evenly spaced *x* values across each site's observed range (9,999 resamples), and the 2.5th and 97.5th percentiles defined the 95% confidence bands.

Effects of year and treatment on ν in the Highfield reversion plots. The effects of year, treatment and their interaction on ν were tested with a two-factor linear model (lm, ν ~ year × treatment). Sums-of-squares were Type III, computed with the *car* package version 3.1-5 under sum-to-zero (effect) coding, providing marginal tests that do not depend on

factor order in an unbalanced design. Effect sizes were expressed as partial eta-squared (η^2_p) with the *effectsize* package version 1.0.3.

Planned contrasts. Estimated marginal means for each year × treatment combination were obtained with *emmeans* version 2.0.4, using the pooled residual variance from the full model. To test whether the conversion of bare fallowed soil to either arable or grassland resulted in an increased ν, each combination was compared with the 2008 fallow mean by a one-sided test, with the alternative that the combination had a higher ν than the 2008 fallow. The resulting probabilities were adjusted across all comparisons by the Benjamini–Hochberg false-discovery-rate procedure.

References

1. Winowiecki, L. A. *et al.* Multistakeholder Engagement to Scale Soil Health Globally: The Coalition of Action 4 Soil Health. *Eur. J. Soil Sci.* **76**, e70128 (2025).
2. Intergovernmental Panel on Climate Change. *Climate Change and Land: IPCC Special Report on Climate Change, Desertification, Land Degradation, Sustainable Land Management, Food Security, and Greenhouse Gas Fluxes in Terrestrial Ecosystems*. (Cambridge University Press, 2022). doi:10.1017/9781009157988.
3. Timmis, K. & Ramos, J. L. The soil crisis: the need to treat as a global health problem and the pivotal role of microbes in prophylaxis and therapy. *Microb. Biotechnol.* **14**, 769–797 (2021).
4. Lehmann, J., Bossio, D. A., Kögel-Knabner, I. & Rillig, M. C. The concept and future prospects of soil health. *Nat. Rev. Earth Environ.* **1**, 544–553 (2020).
5. Sadiq, F. K. *et al.* Conservation Agriculture for Sustainable Soil Health Management: A Review of Impacts, Benefits and Future Directions. *Soil Syst.* **9**, 103 (2025).

6. Khangura, R., Ferris, D., Wagg, C. & Bowyer, J. Regenerative Agriculture—A Literature Review on the Practices and Mechanisms Used to Improve Soil Health. *Sustainability* **15**, 2338 (2023).
7. Guo, M. Soil Health Assessment and Management: Recent Development in Science and Practices. *Soil Syst.* **5**, 61 (2021).
8. Țopa, D.-C., Căpșună, S., Calistru, A.-E. & Ailincăi, C. Sustainable Practices for Enhancing Soil Health and Crop Quality in Modern Agriculture: A Review. *Agriculture* **15**, 998 (2025).
9. Hughes, H. M. *et al.* Towards a farmer-feasible soil health assessment that is globally applicable. *J. Environ. Manage.* **345**, 118582 (2023).
10. Smith, P. *et al.* How to measure, report and verify soil carbon change to realize the potential of soil carbon sequestration for atmospheric greenhouse gas removal. *Glob. Change Biol.* **26**, 219–241 (2020).
11. Shi, Z., Crowell, S., Luo, Y. & Moore, B. Model structures amplify uncertainty in predicted soil carbon responses to climate change. *Nat. Commun.* **9**, 2171 (2018).
12. Yang, J., Li, A., Yang, Y., Li, G. & Zhang, F. Soil organic carbon stability under natural and anthropogenic-induced perturbations. *Earth-Sci. Rev.* **205**, 103199 (2020).
13. Ma, Y. *et al.* Global crop production increase by soil organic carbon. *Nat. Geosci.* **16**, 1159–1165 (2023).
14. Lal, R. Nature-based solutions of soil management and agriculture. *J. Soil Water Conserv.* **77**, 23A-29A (2022).
15. Paustian, K., Larson, E., Kent, J., Marx, E. & Swan, A. Soil C Sequestration as a Biological Negative Emission Strategy. *Front. Clim.* **1**, (2019).
16. Vogel, H.-J. *et al.* A systemic approach for modeling soil functions. *SOIL* **4**, 83–92 (2018).

17. Harris, J. A., Evans, D. L. & Mooney, S. J. A new theory for soil health. *Eur. J. Soil Sci.* **73**, e13292 (2022).

18. Hassan-Dalléac, S., Guiga, W. & Suau-Pernet, A. Soil microbes are the tiny bioengineers running Earth's underground factory. *Commun. Earth Environ.* **7**, 403 (2026).

19. Hartmann, M. & Six, J. Soil structure and microbiome functions in agroecosystems. *Nat. Rev. Earth Environ.* 1–15 (2022) doi:10.1038/s43017-022-00366-w.

20. Neal, A. L. *et al.* Soil as an extended composite phenotype of the microbial metagenome. *Sci. Rep.* **10**, 10649 (2020).

21. Bordoloi, S., Ni, J. & Ng, C. W. W. Soil desiccation cracking and its characterization in vegetated soil: A perspective review. *Sci. Total Environ.* **729**, 138760 (2020).

22. Pachepsky, Y. & Hill, R. L. Scale and scaling in soils. *Geoderma* **287**, 4–30 (2017).

23. Young, I. M. & Crawford, J. W. Interactions and Self-Organization in the Soil-Microbe Complex. *Science* **304**, 1634–1637 (2004).

24. Crawford, J. W., Harris, J. A., Ritz, K. & Young, I. M. Towards an evolutionary ecology of life in soil. *Trends Ecol. Evol.* **20**, 81–87 (2005).

25. Crawford, J. W. *et al.* Microbial diversity affects self-organization of the soil–microbe system with consequences for function. *J. R. Soc. Interface* **9**, 1302–1310 (2011).

26. Feeney, D. S. *et al.* Three-dimensional microorganization of the soil-root-microbe system. *Microb. Ecol.* **52**, 151–158 (2006).

27. Young, I. M., Crawford, J. W., Nunan, N., Otten, W. & Spiers, A. Microbial Distribution in Soils: Physics and Scaling. in *Advances in Agronomy, Vol 100* (ed. Sparks, D. L.) vol. 100 81–121 (Elsevier Academic Press Inc, San Diego, 2008).

28. Marković, D. & Gros, C. Power laws and self-organized criticality in theory and nature. *Phys. Rep.* **536**, 41–74 (2014).

29. Bak, P., Tang, C. & Wiesenfeld, K. Self-organized criticality. *Phys. Rev. A* **38**, 364–374 (1988).

30. Rivera, A. L., Toledo-Roy, J. C. & Frank, A. Symmetry and Signs of Self-Organized Criticality in Living Organisms. *J. Phys. Conf. Ser.* **1612**, 012024 (2020).

31. Stauffer, D. Scaling theory of percolation clusters. *Phys. Rep.* **54**, 1–74 (1979).

32. Soto-Gómez, D. *et al.* Percolation theory applied to soil tomography. *Geoderma* **357**, 113959 (2020).

33. Jarvis, N., Larsbo, M. & Koestel, J. Connectivity and percolation of structural pore networks in a cultivated silt loam soil quantified by X-ray tomography. *Geoderma* **287**, 71–79 (2017).

34. Scheffer, M. *et al.* Early-warning signals for critical transitions. *Nature* **461**, 53–59 (2009).

35. Neal, A. L. *et al.* Arable soil nitrogen dynamics reflect organic inputs via the extended composite phenotype. *Nat. Food* **4**, 51–60 (2023).

36. Hirsch, P. R. *et al.* Soil resilience and recovery: rapid community responses to management changes. *Plant Soil* **412**, 283–297 (2017).

37. Johnston, A. E., Poulton, P. R. & Coleman, K. Chapter 1 Soil Organic Matter. in *Advances in Agronomy* vol. 101 1–57 (Elsevier, 2009).

38. Hawkins, J., Griffith, B., Sint, H. & Harris, P. The North Wyke Farm Platform: Design, Establishment and Development. https://doi.org/10.23637/ROTHAMSTED.98Y1X (2023) doi:10.23637/ROTHAMSTED.98Y1X.

39. Xu, X., Wang, J., Lv, J.-P. & Deng, Y. Simultaneous analysis of three-dimensional percolation models. *Front. Phys.* **9**, 113–119 (2014).

40. Harter, T. Finite-size scaling analysis of percolation in three-dimensional correlated binary Markov chain random fields. *Phys. Rev. E* **72**, 026120 (2005).

41. Johannes, A. *et al.* Optimal organic carbon values for soil structure quality of arable soils. Does clay content matter? *Geoderma* **302**, 14–21 (2017).

42. Fukumasu, J., Jarvis, N., Koestel, J., Kätterer, T. & Larsbo, M. Relations between soil organic carbon content and the pore size distribution for an arable topsoil with large variations in soil properties. *Eur. J. Soil Sci.* **73**, e13212 (2022).

43. Rappoldt, C. & Crawford, J. W. The distribution of anoxic volume in a fractal model of soil. *Geoderma* **88**, 329–347 (1999).

44. Zhang, X. *et al.* Relationship between soil carbon sequestration and the ability of soil aggregates to transport dissolved oxygen. *Geoderma* **403**, 115370 (2021).

45. Network resilience - ScienceDirect. https://www.sciencedirect.com/science/article/pii/S0370157322001211?via%3Dihub.

46. The Long Term Experiments. *Rothamsted Research* https://www.rothamsted.ac.uk/long-term-experiments.

47. Lin, J., Chen, H. & Liu, L. Impact of polydispersity of particle shape and size on percolation threshold of 3D particulate media composed of penetrable superellipsoids. *Powder Technol.* **360**, 944–955 (2020).

48. Poeplau, C. & Don, A. A simple soil organic carbon level metric beyond the organic carbon-to-clay ratio. *Soil Use Manag.* **n/a**,.

49. Powlson, D. S. *et al.* The potential to increase soil carbon stocks through reduced tillage or organic material additions in England and Wales: A case study. *Agric. Ecosyst. Environ.* **146**, 23–33 (2012).

50. Kopittke, P. M. *et al.* The role of soil in defining planetary boundaries and the safe operating space for humanity. *Environ. Int.* **146**, 106245 (2021).

51. Hogan, D. THE SOILS OF NORTH WYKE AND ROWDEN.

52. The <fc>N</fc>orth <fc>W</fc>yke <fc>F</fc>arm <fc>P</fc>latform: effect of temperate grassland farming systems on soil moisture contents, runoff and associated water quality dynamics - Orr - 2016 - European Journal of Soil Science - Wiley Online Library. https://bsssjournals.onlinelibrary.wiley.com/doi/10.1111/ejss.12350.

53. Hawkins, J., Beaumont, D., Sint, H. & Harris, P. *The North Wyke Farm Platform: Field Survey Data*. https://repository.rothamsted.ac.uk/id/eprint/32697/ (2023) doi:10.23637/rothamsted.98y51.

54. Hawkins, J., Griffith, B., Sint, H. & Harris, P. The North Wyke Farm Platform: Design, Establishment and Development. https://doi.org/10.23637/ROTHAMSTED.98Y1X (2023) doi:10.23637/ROTHAMSTED.98Y1X.

55. Livestock Performance for Sheep and Cattle Grazing Lowland Permanent Pasture: Benchmarking Potential of Forage-Based Systems. https://www.mdpi.com/2073-4395/9/2/101.

56. Schneider, C. A., Rasband, W. S. & Eliceiri, K. W. NIH Image to ImageJ: 25 years of image analysis. *Nat. Methods* **9**, 671–675 (2012).

57. Vogel, H. J. & Kretzschmar, A. Topological characterization of pore space in soil — sample preparation and digital image-processing. *Geoderma* **73**, 23–38 (1996).

58. Vogel, H.-J., Weller, U. & Schlüter, S. Quantification of soil structure based on Minkowski functions. *Comput. Geosci.* **36**, 1236–1245 (2010).

59. Wang, M. *et al.* Global soil profiles indicate depth-dependent soil carbon losses under a warmer climate. *Nat. Commun.* **13**, 5514 (2022).

60. Bacq-Labreuil, A. *et al.* Effects of cropping systems upon the three-dimensional architecture of soil systems are modulated by texture. *Geoderma* **332**, 73–83 (2018).

61. Rothamsted Research. Broadbalk soil organic carbon content 1843-2015. 73 KB, 35 KB Electronic Rothamsted Archive, Rothamsted Research https://doi.org/10.23637/KEYREFOABKSOC-02 (2021).

62. R Core Team. (2025) R A Language and Environment for Statistical Computing. R Foundation for Statistical Computing. - References - Scientific Research Publishing. https://www.scirp.org/reference/referencespapers?referenceid=3967248.

63. Warton, D. I., Wright, I. J., Falster, D. S. & Westoby, M. Bivariate line-fitting methods for allometry. *Biol. Rev.* **81**, 259–291 (2006).

64. Krzanowski, W. J. Principal Component Analysis in the Presence of Group Structure. *J. R. Stat. Soc. Ser. C Appl. Stat.* **33**, 164–168 (1984).